Myriocin remodels sphingolipids and modulates proteostasis networks to enhance longevity

Nathaniel L. Hepowit[1], Eric Blalock[2], Sangderk Lee[3], Jason A. MacGurn[1], Robert C. Dickson[4]

[1]Department of Cell and Developmental Biology, Vanderbilt University, Nashville, TN 37240, USA
[2]Department of Pharmacology & Nutritional Science, University of Kentucky, Lexington, KY 40536, USA
[3]Sanders-Brown Centers on Aging, University of Kentucky, Lexington, KY 40536, USA
[4]Department of Molecular and Cellular Biochemistry, University of Kentucky, Lexington, KY 40536, USA

Correspondence to: Robert C. Dickson, Jason A. MacGurn; email: bobd@uky.edu, jason.a.macgurn@vanderbilt.edu

Key words: longevity, ubiquitin, proteostasis, amino acid transport, sphingolipids, lifespan

ABSTRACT

The increasing elderly population is casting a heavy burden on healthcare due to chronic, age-associated diseases. Nutrient limitation is well known to slow the aging process and improve health. Regrettably, practicing nutrient restriction to improve health is unachievable for most people. Alternatively, pharmacological strategies are being pursued including myriocin which increases lifespan in budding yeast. Myriocin impairs sphingolipid synthesis, resulting in lowered amino acid pools which aid entry into a quiescent, long-live state. Here we present transcriptomic data during 6 h of drug treatment that improve our mechanistic understanding of what myriocin does to promote longevity. Specifically, we present a new role for ubiquitin in longevity. Previously we found that the methionine transporter, Mup1, traffics to the plasma membrane normally in myriocin-treated cells but is not active and is endocytosed sooner than in untreated cells. We now show that Mup1 tagged with a deubiquitinase domain (DUB domain) blocks myriocin-enhanced longevity. Although proteostasis and the role of ubiquitin in it are hallmarks of aging, our finding that deubiquitinating an amino acid transporter is vital for longevity in Myriocin-treated cells is novel. Understanding the role of deubiquitination in longevity has the potential to identify new strategies and targets for promoting healthy aging.

INTRODUCTION

Aging is widely accepted as a major risk factor for many chronic diseases and resultant physiological decline leading to mortality [1]. Research on many fronts is revealing potential ways to postpone age-related decline, maintain normal physiological function longer and improve healthspan. Some of the most promising research seeks to limit nutrient intake or increase daily fasting time as a means to improve healthspan in humans [2-4]. Still, these strategies will be difficult for most humans to adhere to in order to gain health benefits. Pharmacological agents offer a potential way to obtain the beneficial effects of nutrient limitation, but such compounds have yet to be identified although progress is encouraging [1, 5, 6].

We have identified a potential pharmacological agent, the natural product myriocin (Myr, ISP-1), that increases chronological lifespan in budding yeasts (*Saccharomyces cerevisiae*) by more than two-fold [7]. Myr works, at least in part, by reducing the free pool of most amino acids similar to what amino acid restriction does [5, 8, 9]. Our interest in Myr stems from its target enzyme serine palmitoyltransferase (SPT), catalyzing the first and rate limiting step in sphingolipid biosynthesis in all eukaryotes [10-12]. In addition, Myr was first identified in a search for antibiotics [13] and anti-inflammatory drugs [14]. More recently, it has shown beneficial effects in treating age-associated diseases including diabetes, cancers, neurological and cardiovascular disorders [15-20] and other diseases including muscular dystrophies, cystic fibrosis and retinopathy [21-23]

Sphingolipids serve as both structural components of cellular membranes and as signal or regulatory molecules influencing many physiological processes, particularly in mammals [15, 24-26]. Because most de novo lipid biosynthesis begins in the endoplasmic reticulum and continues in the Golgi Apparatus before the terminal products are distributed to cellular membranes, Myr treatment has the potential to diminish or enhance a variety of processes. Our recent studies identified diminished processes that may foster longer lifespan: newly synthesized Mup1, the major high-affinity methionine (Met) transporter, trafficked normally to the plasma membrane (PM) but was inactive in drug-treated cells resulting in reduced Met uptake as the fraction of active Mup1 was diluted by cell growth and division. Moreover, Mup1 clearance from the PM began earlier in Myr-treated cells than in untreated cells [7]. Thus, post-translational effects are vital to drug-induced down-sizing of amino acid pools.

Previously we found that Myr treatment had large, global effects on transcription after 6-7 cell doublings [27]. In the present work, we examined mRNA levels during the initial stages of Myr treatment to construct an overview of transcriptional changes with the aim of identifying how long it takes cells to respond to drug treatment and to determine if transcription plays a prominent role in lowering amino acid pools. Additionally, we sought to identify novel factors critical for Myr-enhanced lifespan. We find that very few transcripts respond to Myr in the first 4 h of treatment, but thereafter transcription is strongly up-regulated. We find no indication of transcription having a prominent role in maintaining low amino acid pools in Myr-treated cells. However, transcript data suggested a novel role for ubiquitin in lifespan and targeted studies identified deubiquitination of Mup1 as essential for Myr-enhanced longevity.

RESULTS.

Four hours of myriocin treatment induce robust transcriptional changes

To examine transcriptional changes induced by Myr treatment, we diluted stationary phase cells (50-60% in G_o or quiescent, Q, phase) into fresh culture medium (Time 0), with and without Myr treatment. Samples for analysis of mRNA abundance by RNA seq were taken at 1 h intervals over a 6 h time course (Figure 1A). Data for the zero time were omitted from this analysis because of bias in library sizes which were smaller than expected if most genes were not differentially expressed. The normalized RNA seq data for the 1-6 h time course contained transcripts, expressed as transcripts per million (TPM), mapped to 6198 genes, 5169 of which were uniquely annotated and of sufficient signal intensity for subsequent analysis (Supplementary File 1). Filtered data were analyzed by two-way ANOVA with a statistical cutoff of $\rho = \leq 0.01$ to give a set of 4964 significant genes (Figure 1B). These were further sorted into

drug (D), time (T), both drug and time (DxT) and interactions (TxDxI) (Figure 1C, Venn diagram).

We analyzed the 1254 genes in the TxDxI group at each time point for statistically significant changes (criteria- $p \leq 0.05$ Fisher's protected Least Significant Difference pairwise contrast-pLSD, and fold change ≥ 2) (Supplementary File 2). A notable result is that few genes are up-regulated until the 5 and 6 h time points and very few genes are down-regulated at any time point (Figure 1D). As we discuss in detail below, up-regulation of genes starting between the 4^{th} and 5^{th} h occurs when the majority of cells enter their second cell division cycle. Thus, these data explain much of the effect of time and drug components of the interaction gene set.

We recently reported that Myr treatment has a notable effect on the size of most amino acid pools which remain significantly smaller in drug-treated cells [7]. To determine if transcription has roles in lowering amino acid pools and to gain a global view of significant features of the transcriptome, we performed a gene ontology (GO) analysis of genes in the TxDxI sector of the Venn diagram. GO terms Membrane and Plasma Membrane are highly enriched (Figure 1E), consistent with Myr slowing synthesis of sphingolipids along with synthesis of other lipids and membrane-bound proteins in the ER and consequent remodeling of membrane composition throughout the cell. Other high scoring terms include Actin Cortical Patch, indicating membrane growth and remodeling as well as cell grow and division. The term Oxidation-Reduction Process primarily identifies chemical reactions in metabolic pathways which are captured also by the KEGG pathway term Metabolic Pathways. Lastly, Endocytosis, another high ranking KEGG pathway, has functional links to the terms Membrane, Plasma Membrane and Actin Cortical Patch and to Mup1, the major methionine transporter, presented below.

Enriched GO terms in three other sectors of the Venn diagram (Figure 2A) were analyzed starting with genes listed in columns labeled Time x Drug and Time (Figure 2B). Our focus was on genes matching one of the 10 indicated patterns over the 1-6 h time-frame. Patterns were sorted into ones having transcripts that behaved like the diagramed pattern or like its mirror image (+ or –, respectively, as indicated in the column labeled 'Corr'). Only patterns showing significantly more genes (indicated by an asterisk, binomial test $\rho \leq 0.05$) assigned to them than expected by chance were analyzed. Most enriched GO terms in the Time x Drug group represent processes requiring many genes including cell growth and division (Figure 2C). The genes and GO terms present in all of the patterns analyzed are shown in Supplementary File 2. A graph of any gene transcript across the 1-6 h time-frame can be plotted using the Graph Reporter tab in Supplementary File 1.

In contrast to the Time x Drug sector, the 1009 genes in the Time sector of the Venn diagram fall into multiple patterns with the B1 and B10 patterns being most highly represented. Genes in this sector are not significantly changed by Myr but are significantly changed with time and serve as an example of time-related changes. All of these patterns will require further effort to determine their significance in Myr-induced longevity.

The Drug sector of the Venn diagram contains 401 genes with most (329, Supplementary File 2) being up-regulated. As expected, these genes do not strongly associate with any temporal pattern (Figure 2B, right-most column). However, these genes do respond to Drug but not to Time. Because of our experimental design, we cannot be sure if some genes in this sector are driving the changes we see that are associated with time but they could be. The most enriched GO terms are Regulation of Transcription, DNA Templated and Nucleus (Figure 2E), indicating a strong response to Myr treatment independent of time in culture.

In summary, GO term analysis of transcriptional changes in ten patterns during the 1-6 h time course of Myr treatment gives little indication of transcriptional involvement in keeping amino acid pools low in drug-treated cells. If there is a contribution, it may be overlooked because the number of genes involved is too small to achieve statistical significance at the pathway level, or transcriptional changes do not fall into any of the 10 patterns we examined.

Correlation analysis of transcriptomics data identifies clues to amino acid metabolism

As another approach to understand effects of Myr on the transcriptome, we analyzed transcript data using the R program package of Weighted Gene Correlation Network Analysis, WGCNA [28], to identify clusters (modules) of highly correlated genes showing a similar response to Myr over the 1-6 h time course. A gene dendrogram produced by average linkage of hierarchical clustering revealed many modules with the seven most correlated having from 18 to 2490 genes (Supplementary File 3, column L). Examination of the relationship of the modules to free amino acid pools over time identified the Brown and Green modules with 1126 and 144 genes, respectively, as having a negative correlation to Myr treatment: Myr maintains low pool levels but enhances the level of a transcript at one or more time points (Figure 3A). A network representing the relationship between genes in the Brown and Green modules includes the Turquoise module whose genes interact with both the Brown and Green modules (Figure 3B).

Such negative correlation in a module is exemplified by an Eigengene representing the average effect of Myr on genes compared to the untreated drug control (Supplementary File 4). For example, the Eigengene representing the Brown module shows that Myr induces transcription starting at 4 h (Figure 3C) whereas there is no increase in amino acid pool size in drug-treated cells [7]. The highest-ranking GO term in the Brown module is Regulation of Transcription where drug treatment enhances transcript levels particularly after 4 h, consistent with the ANOVA analysis represented in Figure 1D. A different negative correlation is seen for the Eigengene representing the small Green module where genes are up-regulated by Myr from 1-4 h and then drop below values in untreated cells (Figure 3E). The main GO term in the Green module is Translation (Biological Process, p = 1.7E-88) along with Ribosome Assembly and related processes responding to drug-induced slowing of protein synthesis and growth rate [7]. Lastly, the large Turquoise module with 2490 genes captures Myr-induced transcriptional events involving processes or pathways or cell components each with more than 200 genes (Figures 3F and 3G). Interestingly, transcripts represented in the Turquoise module rapidly increases after 4 h of drug treatment, substantiating the ANOVA analysis represented in Figure 1D. Substantial effort will be required to delineate the contribution of these genes to Myr-enhanced longevity.

Deubiquitination of Mup1 is essential for Myr-enhanced longevity

A drawback of WGCNA and pathway and pattern analyses is a reduced ability to identify significant biological features involving smaller numbers of genes or for genes that do not fit a specific pattern across the 1-6 h time-frame. To circumvent these limitations and to discover transcript changes with potential roles in lowering amino acid pools, we examined genes with the highest possible significance (1E-16) in the Drug, Time and Interactions columns of data from the two-way ANOVA analysis of mRNA levels. This approach identified only 16 genes out of the 4964 genes (Supplementary File 1, Filter Tab, columns M, N and O). The *UBI4* gene encoding the major stress-associated ubiquitin captured our attention because stresses of various types have known roles in aging and longevity and we previously identified stress responses in Myr-treated cells [27, 29]. A defining feature of *UBI4* transcript abundance is a rapid increase over the 4-6 h time period (Figure 4A), corresponding to the time when Myr has

its most significant effect on transcription (Figure 1D). The trajectory of *UBI4* transcripts appear to be like transcript pattern B4 with 150 genes up-regulated between 4-5 h in the Time x Drug column of Figure 2B. The highest-ranking GO term in this group of genes is Protein Monoubiquitination (Figure 2C): Protein Polyubiquitination is also found at a lower significance level in this group. However, due to the stringent nature of ANOVA analysis, the *UBI4* transcript does not fit in the B4+ pattern. But it does fits into a unique pattern containing 72 genes (Supplementary File 5). Importantly, the GO terms Protein Monoubiquitination and Protein Polyubiquitination are also enriched in this group. The potential biological significance of the *UBI4* transcript pattern may relate to our previous analyses of Mup1-pHluorin trafficking. We found that the fluorescent signal decreases from the PM more rapidly, 4-7 h time-frame, in Myr-treated cells in a dose-dependent manner and requires ubiquitin conjugation for endocytosis to occur [7].

To determine if ubiquitination has roles in Myr-enhanced CLS, we examined untreated *ubi4*Δ cells and found a faster loss of viability compared to BY4741 cells (Figure 4B, 50% survival day 3 vs day 5, respectively). For Myr-treated cells, 50% survival occurred on day 3-4 for *ubi4*Δ cells vs day 10 for BY4741 cells. Around the 50% survival point, drug-treated *ubi4*Δ cells appear to survive slightly longer than untreated cells, suggesting a small effect of Myr on lifespan. Since ubiquitin has many functions, we studied its role in endocytosis of Mup1 using the same strains as used in our published analyses of endocytosis [7]. Specifically, CLS was assayed using cells with chromosomal *MUP1* tagged with pHluorin-UL36 (catalytic active or catalytic dead, CD). UL36 is a viral deubiquitinase (DUB) that can reverse localized ubiquitin conjugation activity, thus protecting the fusion protein from ubiquitin-mediated degradation or trafficking events [30]. We find that while Mup1-UL36 blocks Myr-enhancement of CLS (Figure 4C, dashed blue curve) strains lacking the UL36 fusion (dashed black curve) or isogenic strains containing the catalytic dead variant (UL36-CD; dashed magenta curve) do not interfere with Myr-induced longevity. To establish that deubiquitination is required for drug-enhanced longevity rather than just the lack of Mup1 transport activity, we analyzed *mup1Δ* cells. Myr treatment enhanced CLS in *mup1Δ* cells like it does in BY4741 cells and in control cells in which the *MUP1* wild-type allele has been used to replace the mutant chromosomal *mup1Δ* allele (Figure 4D, compare dashed lines). We conclude from these data that removal of ubiquitin from Mup1 is essential for Myr-induced longevity.

DISCUSSION

We performed transcriptomics analysis for several reasons including (i) to determine if transcription played roles in keeping amino acid pools at a low level in Myr-treated cells, (ii) to determine if Myr treatment caused a major transcriptional shift during a specific time-frame and (iii) to search for novel processes or pathways required for Myr-enhanced longevity. Amino acid pools are lower in Myr treated cells compared to untreated cells after 1 h of treatment [7]. We did not identify any indication that initial amino acid pool lowering s driven by transcription. However, we cannot eliminate possible effects on some amino acid pools. We were able to determine when cells begin responding to drug treatment under our assay conditions (Figure 1A). Transcripts (genes) changing in a statistically significant way across the initial 6 h of Myr treatment were identified by two-way ANOVA analysis (Figure 1B). Significant genes were sorted into ones responding primarily to Time (T) or Drug (D) or Interaction (I) (Figure 1C). To generate an overview of drug effects over time, we examined the 1254 genes in the TxDxI group at each time point for genes with 2-fold changes greater or less than 1 (Figure 1D). Surprisingly, very few transcripts that are significant by Interaction respond to Myr until after 4 h of treatment which, for the majority of cells, occurs after the first cell division (during the second

cell division cycle). The major GO terms in the TxDXI sector of the Venn diagrams reflect processes, reactions and compartments related to cell growth and division (Figure 1E). The large upsurge of transcripts after 4 h of Myr-treatment along with the cellular processes and compartments they represent was also identified by correlation analysis as visualized by the Eigengene for the Brown and Turquoise modules (Figures 3C and 3F). The Turquoise module being especially significant as it contains nearly half of all transcripts identified as significant by two-way ANOVA analysis (Figure 1A). Our data probably underestimate the number of significant genes at each time point since only 50-60% of cells are acting in synchrony [7] or that temporal blurring distorted temporal assignment. Nonetheless, this is not likely to change our conclusion that Myr causes its greatest effects on transcription after about 4 h of treatment or after cells have executed their first cell division.

Possible future studies to better understand Myr-effects on amino acid and other types on metabolism are implicated by our transcriptomics data. The GO term Metabolic Pathways (193 genes) was identified in the Interaction analysis as being highly significant across the 1-6 h time-frame (Figures 1D and 1E). GO term analysis of these 193 genes identified KEGG pathways for carbon metabolism, secondary metabolites, amino acid metabolism (tryptophan, methionine, lysine, arginine, proline, histidine) and other types of metabolism as being significantly enriched (Supplementary File 2, Tab “TxDxI 1254”). Several of these pathways have known roles in longevity (e.g. Glycogen and Trehalose metabolism), suggesting that the Myr-sensitive pathways defined in this work are novel but include elements of pathways defined in prior work as having roles in longevity. Endocytosis is another GO term found to be highly enriched in the Interaction analysis of transcripts across the 1-6 h time-frame (Figures 1D and 1E). GO term analysis of this group of 39 genes shows enrichment for genes involved in ubiquitin-mediated endocytosis which provide clues for the proteins, lipids and cellular machinery controlling Myr-induced endocytosis of Mup1 that we previously observed [7]. The 39 genes in this group will facilitate understanding the cellular processes controlled by Myr that depend on ubiquitin and deubiquitination of Mup1 involved in Myr-enhanced lifespan (Figures 4B and 4C).

To uncover processes, pathways or cellular compartment related to removal of amino acid transporters like Mup1 from the PM, we examined genes with the highest statistical significance (E1-16) from the ANOVA analysis of the Time and Drug and Interaction columns because genes meeting these criteria would be more likely to have a genuine role in Myr-enhance longevity, yet they might not standout as significant using pathway or correlation analyses, especially if their expression patterns are unique. One gene, *UBI4*, in this group of 16 genes stood out because of its potential to be essential for removal of Mup1 and other proteins from the PM and to be vital for Myr-enhanced longevity. Indeed, the Ubi4 protein proved to be required for drug-induced longevity since deleting the gene blocked Myr-enhancement of lifespan (Figure 4B). In addition, tagging Mup1 with the UL36 deubiquitination domain blocked Myr-enhanced longevity (Figure 4B). A potential limitation of our data is the possibility of the UL36 deubiquitinase domain having proximal effects on proteins in the vicinity of the Mup1-pHluorin-UL36 protein [30, 31]. Futures studies will be required to evaluate if such proximal effects are involved in the impairment of Myr-enhanced lifespan. Also, additional amino acid transporters tagged with a UL36 domain will need to be examined to determine if they impair Myr-enhancement of longevity like UL36-tagged Mup1 does. The outcomes of these studies will potentially provide a novel avenue to enhancing longevity and new targets or strategies for improving human healthspan.

MATERIAL AND METHODS

Strains, culture conditions, lifespan assays and statistical significance

Strains (Table 1), culture conditions, lifespan assays and their statistical significance were similar to ones described previously [7]. CLS assays were performed at least twice using triplicate cultures. Concentrations of Myr used in CLS assays ranged from 475-525 ng/ml depending on the sensitive of strains compared to wild-type, prototrophic BY4741. Drug-sensitivity was measured by culture density (A600nm) after 24 h of growth using cultures started at 0.15 A600nm units of cells/ml. All BY4741 yeast strains used for lifespan assays and for RNA extraction were made prototrophic by transformation with the pHLUM plasmid (Addgene, Watertown, Massachusetts) [32]. The DUB (UL36) fusion yeast strains used in this study were generated by homologous recombination in BY4741 and SEY6210 background strains using the reagents and strategy previously described (Hepowit et al. 2022). The *MUP1* knock-in strain (NHY945) was generated in BY4741 by swapping the endogenous *MUP1* coding region with NATMX (NHY930), shuffling the chromosomally integrated *NATMX* with *URA3* (NHY938.1), and snipping out *URA3* by homologous reintegration of a PCR-amplified *MUP1* coupled with counter selection on 5-fluoroorotic acid (5-FOA) synthetic media plate.

Budding yeast mRNA-enriched profiles from 42 individual samples of prototrophic BY4741 cells, including 3 replicates of 7 time points and 2 treatments (control and drug-treated) were used. Culture conditions were similar to ones described previously (Hepowit et al. 2021, Aging) except for the following modifications. Prototrophic BY4741 yeast cells were grown in 200 ml of SDC culture medium in a 1 L flask with the medium heated to 30°C before addition of EtOH (final concentration of 0.3% (control samples). For drug-treated samples, myriocin was added after addition of EtOH to give final concentrations of 0.3 % EtOH and 700ng/ml myriocin. Lastly, cells from a saturated overnight culture were diluted into the 200 ml cultures to give an initial A600nm units/ml of 0.15. Flasks were incubated at 30°C and 200 rpm on a rotary shaker. Control cells (containing final concentration of 0.3% EtOH) and myriocin-treated cells (final concentrations of 0.3 % EtOH and 700ng/ml myriocin) were harvested at time 0, 1, 2, 3, 4, 5 and 6 hours (all time points for each replication from the same culture flask).

RNA extraction

RNA was extracted from 5 A600nm unit/ml of yeast cells, filtered at time 0 and then every h up to 6 h on a membrane filter, as described previously for amino acid extraction [7]. Filtered cells were washed once with 5 ml of ice-cold nanopure water and the filter was quickly transferred to a chilled 1.5 ml microfuge tube containing 0.5 ml cold nanopure water. Tubes were vortexed 10 sec followed by centrifugation for 15 sec. Supernatant fluid (450 µl) was transferred to a new tube and frozen in a dry-ice EtOH bath followed by storage at -80°C. Cold acid-washed glass beads (300 µl, 0.5 mm dia.) were added to a frozen cell pellet followed by addition of 300 µl of RLT buffer (RNAeasy mini kit, Qiagen, Germantown, Maryland). Tubes were vortexed 5 min at room temperature and placed on ice for 1 min. This cycle was done 4 times followed by addition of 300 µl of ice-cold RLT buffer, mixing, and centrifugation at 13,000xg for 2 min at room temperature. Supernatant fluid (450 µl) was transferred to a new microfuge tube and then mixed with 1 ml of 70% EtOH before transfer to a RNeasy spin column and processed according to the manufacturer's instructions. Processed samples were frozen in a dry-ice EtOH bath and stored at -80°C. RNA seq was performed on total RNA samples at the Roy J. Carver Biotechnology Center at the University of Illinois.

RNA seq analysis

RNA sequencing was performed on total RNA samples at the Roy J. Carver Biotechnology Center at the University of Illinois. Two different mixes of ERRC spike-in RNA controls were added to the samples; one mix for the control samples, and one mix for the drug-treated samples. Libraries were constructed with Illumina's 'TruSeq Stranded mRNAseq Sample Prep kit'. Each library was quantitated by qPCR and sequenced on one lane for 151 cycles from each end of the fragments on a HiSeq 4000 using a HiSeq 4000 sequencing kit version 1. Fastq files were generated and demultiplexed with the bcl2fastq v2.17.1.14 Conversion Software (Illumina). Each sample's pair of fastq files were run through trimmomatic 0.36 to first remove any remaining standard Illumina PE v3 adapters, then trim bases from both ends with quality scores below 28, and finally to remove individual reads shorter than 30 bp and their paired read, regardless of length (parameters ILLUMINACLIP:/home/apps/trimmomatic/trimmomatic-0.36/adapters/TruSeq3-PE.fa:2:15:10 TRAILING:28 LEADING:28 MINLEN:30). Paired reads per sample were pseudo-aligned to the Yeast R64 transcriptome and 92 ERRC spike-in control sequences using Salmon 0.8.2 with parameters -l A --numbootstraps=30 --seqBias –gcBias. Resulting FASTQ files mapped to the yeast genome (R64), resulted in count files and normalized using the transcripts per million (TPM) algorithm [33] using WebMev [34]. Resulting data were downloaded as flat files and loaded into Excel for further analysis. From a total of 6198 mapped genes, 5169 were uniquely annotated with gene symbols and had sufficient non-zero readings for further analysis. The filtered data were analyzed by two-way ANOVA for the main effects of drug and time, as well as for interaction. Significant by the time term or both the drug and time term, data were further analyzed by post-hoc pairwise Fisher's protected Least Significant Difference (pLSD), and log 2-fold change comparison to further isolate the effects of drug over time. Template analysis was applied using pre-determined templates (depicted in Fig. 2) correlated to average expression over time in drug or control conditions. Each gene significant by time and/or interaction was correlated to each of the ten templates and was assigned to the template with which it had the strongest correlation. Data have been deposited in the GEO (GSE199904) [NCBI tracking system #22817261].

Gene regulatory network using WGCNA

The WGCNA (v1.70-3) [28] was used to identify gene modules and build unsigned co-expression networks, which include negative and positive correlations. Briefly, WGCNA constructs a gene co-expression matrix, uses hierarchical clustering in combination with the Pearson correlation coefficient to cluster genes into groups of closely co-expressed genes termed modules, and then uses singular value decomposition (SVD) values as module eigengenes to determine the similarity between gene modules or to calculate association with sample traits (for example, incubation time or amino acid levels). The top 2,000 variable genes were used to identify gene modules and network construction. Soft power 8 was chosen by the WGCNA function pick SoftThreshold. Then, the function TOMsimilarityFromExpr was used to calculate the TOM similarity matrix via setting power = 8, networkType = "signed. The distance matrix was generated by subtracting the values from similarity adjacency matrix by one. The function flashClust (v.1.01) was used to cluster genes based on the distance matrix, and the function cutreeDynamic was utilized to identify gene modules by setting deepSplit =3. Cytoscape (v.3.8.2) was applied for the network visualizations.

FIGURE LEGENDS

Figure 1. Summary of transcriptomics data analysis. (A) Outline of experimental design for collecting cells, treated or not treated with Myr, for analysis of mRNAs by RNA seq. (B) Overview of RNA seq data analysis by two-way ANOVA. (C) Venn diagram summarizing the

results of the ANOVA analysis for Drug, Time and Interaction. (D) Diagram summarizing analysis of the 1254 genes in the Interaction group of the Venn diagram for ones with log 2-fold changes greater than 1 for p-values ≤ 0.05 (pairwise pLSD) at each hourly time point. (E) Pathway overrepresentation analysis was performed with DAVID [35] using Gene Ontology (GO) [36] analysis of the 1254 genes in the Interaction group. All data for the 5169 RNA seq transcripts that passed filtering metrics are shown in Supplementary File 1 which also contains the two-way ANOVA results and can be used to sort for genes in each sector of the Venn diagram.

Figure 2. Detailed analysis of the Drug, Time and Drug x Time components of the transcriptomics data set identified by two-way ANOVA analysis. (A) Diagram of two-way ANOVA analysis with results summarized in a Venn diagram showing the number of genes in each sector and indicating the three groups of genes (Time, Time x Drug and Drug) that were analyzed further for ones matching specific patterns. (B) Summary of genes matching the 10 indicated patterns. The column labelled “Corr” indicates genes having the same time course (+) or the inverse (mirror image) time course (-) of a pattern. Columns labeled Time, Time x Drug and Drug indicate the number of genes matching the corresponding pattern or its mirror image. Arrows at the top of the columns indicate genes up or down-regulated by drug. Statistically significant groups of genes are indicated by bold fond and with an asterisk (*). (C) Summary of top enriched GO terms found in specific patterns. Genes and GO analysis of groups indicated by an asterisk are listed in Supplementary File 2.

Figure 3. Correlation analysis of transcriptomics data. (A) The 7 color-coded modules whose gene members are highly correlated over time (left-hand side of diagram) were analyzed for their relationship to each amino acid pool (pool data are from [7]). The degree of correlation is indicated by the red-green (correlated-anticorrelated) scale at the right-side of the diagram. This figure indicates that the Green and Brown modules are the most anti-correlated (red shading) with amino acid pool, most of which are lowered by Myr treatment (right-most column labeled “myriocin” at the bottom of the diagram). Thus, genes in the Green module are up-regulate by myriocin treatment whereas pool size is down regulated. (B) Network diagram showing the relationship of genes in the Green and Brown modules which are connected by genes in the Turquoise. Genes are indicated by Nodes (circles) and relationships by edges. All genes and relationship values are presented in Supplementary File 3. (C) Scatter plot of the Brown Eigengene across the 1-6 h time frame. (D) Enriched GO terms found in the Brown module. (E) Scatter plot of the Green Eigengene across the 1-6 h time. (F) Scatter plot of the Turquoise Eigengene across the 1-6 h time frame. (G) Enriched GO terms found in the Turquoise module. Genes used in calculating the mean Eigengene are in Supplementary File 3 and the 7 mean Eigengene values and their scatter plots are presented in Supplementary File 4.

Figure 4. Ubiquitin plays a central role in Myr-enhanced longevity. (A) *UBI4* transcript level across the 1-6 h time frame in Myr-treated or untreated cells. (B) CLS assay showing that *ubi4Δ* mutant cells impair Myr-enhancement of lifespan compared to BY4741 wild-type cells. (C) Data showing that removing ubiquitin from Mup1 is essential for Myr-enhanced lifespan. CLS assays of cells having Mup1-pHlurion tagged with the UL36 deubiquitinase domain (DUB) impair Myr-enhancement of CLS whereas replacing catalytically active UL36 with a catalytically dead UL36 domain (UL36-CD) restores Myr-enhanced lifespan. (D) Control lifespan assay to show that deleting *MUP1* does not impair Myr-enhanced longevity.

Table 1. Strains used in this study

Strain	Genotype	Reference
BY4741	*MATa his3-Δ1 leu2-Δ0 ura3-Δ0 met15-Δ0*	[37]

SEY6210	*MATalpha leu2-2,112 ura3-52 his 3delta200 trp1-delta901 lys2-801 suc2-delta9*	[38]
NHY413	*SEY6210 Mup1-pHluorin::NATMX*	[7]
NHY414	*SEY6210 Mup1-pHluorin::NATMX Vph1-MARS::TRP1*	[7]
NHY447	*SEY6210 Mup1-pHluorin-UL36(N-term 15-260 HSV1 UL36, active)::KANMX*	[7]
NHY431	*SEY6210 Mup1-pHluorin-UL36(N-term 15-260 HSV1 UL36 C40S, inactive)::KANMX*	[7]
RCD2073	BY4741 *MATa his3-Δ1 leu2-Δ0 ura3-Δ0 met15-Δ0 ubi4Δ::KAN*	[39]
NHY415	BY4741 *MATa his3-Δ1 leu2-Δ0 ura3-Δ0 met15-Δ0 Mup1-pHluorin (NATMX)*	This study
NHY425	BY4741 *MATa his3-Δ1 leu2-Δ0 ura3-Δ0 met15-Δ0 Mup1-pHluorin-UL36 (KANMX)*	This study
NHY426	BY4741 *MATa his3-Δ1 leu2-Δ0 ura3-Δ0 met15-Δ0 Mup1-pHluorin-UL36 catalytic dead (KANMX)*	This Study
NHY930	BY4741 *MATa his3-Δ1 leu2-Δ0 ura3-Δ0 Δmup1::NATMX*	This Study
NHY938.1	BY4741 *MATa his3-Δ1 leu2-Δ0 ura3-Δ0 Δmup1::URA3*	This Study
NHY938.2	BY4741 *MATa his3-Δ1 leu2-Δ0 ura3-Δ0 Δmup1::URA3*	This Study
NHY945	BY4741 *MATa his3-Δ1 leu2-Δ0 ura3-Δ0 MUP1 knockin*	This Study

CONFLICTS OF INTEREST

The authors declare that they have no conflicts of interest

REFERENCES

1. Gonzalez-Freire M, Diaz-Ruiz A, Hauser D, Martinez-Romero J, Ferrucci L, Bernier M and de Cabo R. The road ahead for health and lifespan interventions. Ageing research reviews. 2020; 59:101037.
2. Aon MA, Bernier M, Mitchell SJ, Di Germanio C, Mattison JA, Ehrlich MR, Colman RJ, Anderson RM and de Cabo R. Untangling Determinants of Enhanced Health and Lifespan through a Multi-omics Approach in Mice. Cell Metab. 2020; 32(1):100-116 e104.
3. Stekovic S, Hofer SJ, Tripolt N, Aon MA, Royer P, Pein L, Stadler JT, Pendl T, Prietl B, Url J, Schroeder S, Tadic J, Eisenberg T, et al. Alternate Day Fasting Improves Physiological and Molecular Markers of Aging in Healthy, Non-obese Humans. Cell Metab. 2019; 30(3):462-476 e465.
4. Madeo F, Carmona-Gutierrez D, Hofer SJ and Kroemer G. Caloric Restriction Mimetics against Age-Associated Disease: Targets, Mechanisms, and Therapeutic Potential. Cell Metab. 2019; 29(3):592-610.
5. Lee MB, Hill CM, Bitto A and Kaeberlein M. Antiaging diets: Separating fact from fiction. Science. 2021; 374(6570):eabe7365.
6. Tyshkovskiy A, Bozaykut P, Borodinova AA, Gerashchenko MV, Ables GP, Garratt M, Khaitovich P, Clish CB, Miller RA and Gladyshev VN. Identification and Application of Gene Expression Signatures Associated with Lifespan Extension. Cell Metab. 2019; 30(3):573-593 e578.

7. Hepowit NL, Macedo JKA, Young LEA, Liu K, Sun RC, MacGurn JA and Dickson RC. Enhancing lifespan of budding yeast by pharmacological lowering of amino acid pools. Aging. 2021; 13.
8. Green CL and Lamming DW. Regulation of metabolic health by essential dietary amino acids. Mech Ageing Dev. 2019; 177:186-200.
9. Longo VD, Antebi A, Bartke A, Barzilai N, Brown-Borg HM, Caruso C, Curiel TJ, de Cabo R, Franceschi C, Gems D, Ingram DK, Johnson TE, Kennedy BK, et al. Interventions to Slow Aging in Humans: Are We Ready? Aging Cell. 2015; 14(4):497-510.
10. Miyake Y, Kozutsumi Y, Nakamura S, Fujita T and Kawasaki T. Serine palmitoyltransferase is the primary target of a sphingosine-like immunosuppressant, ISP-1/myriocin. Biochem Biophys Res Commun. 1995; 211(2):396-403.
11. Hanada K. Serine palmitoyltransferase, a key enzyme of sphingolipid metabolism. Biochim Biophys Acta. 2003; 1632(1-3):16-30.
12. Dickson RC and Lester RL. Metabolism and selected functions of sphingolipids in the yeast *Saccharomyces cerevisiae*. Biochim Biophys Acta. 1999; 1438(3):305-321.
13. Kluepfel D, Bagli J, Baker H, Charest MP and Kudelski A. Myriocin, a new antifungal antibiotic from Myriococcum albomyces. J Antibiot (Tokyo). 1972; 25(2):109-115.
14. Fujita T, Inoue K, Yamamoto S, Ikumoto T, Sasaki S, Toyama R, Chiba K, Hoshino Y and Okumoto T. Fungal metabolites. Part 11. A potent immunosuppressive activity found in Isaria sinclairii metabolite. J Antibiot (Tokyo). 1994; 47(2):208-215.
15. Quinville BM, Deschenes NM, Ryckman AE and Walia JS. A Comprehensive Review: Sphingolipid Metabolism and Implications of Disruption in Sphingolipid Homeostasis. Int J Mol Sci. 2021; 22(11).
16. Petit CS, Lee JJ, Boland S, Swarup S, Christiano R, Lai ZW, Mejhert N, Elliott SD, McFall D, Haque S, Huang EJ, Bronson RT, Harper JW, et al. Inhibition of sphingolipid synthesis improves outcomes and survival in GARP mutant wobbler mice, a model of motor neuron degeneration. Proc Natl Acad Sci USA. 2020; 117(19):10565-10574.
17. Woo CY, Baek JY, Kim AR, Hong CH, Yoon JE, Kim HS, Yoo HJ, Park TS, Kc R, Lee KU and Koh EH. Inhibition of Ceramide Accumulation in Podocytes by Myriocin Prevents Diabetic Nephropathy. Diabetes Metab J. 2019; 44(4):581-591.
18. Piano I, D'Antongiovanni V, Novelli E, Biagioni M, Dei Cas M, Paroni RC, Ghidoni R, Strettoi E and Gargini C. Myriocin Effect on Tvrm4 Retina, an Autosomal Dominant Pattern of Retinitis Pigmentosa. Front Neurosci. 2020; 14:372.
19. Lin G, Wang L, Marcogliese PC and Bellen HJ. Sphingolipids in the Pathogenesis of Parkinson's Disease and Parkinsonism. Trends Endocrinol Metab. 2019; 30(2):106-117.
20. Tippetts TS, Holland WL and Summers SA. Cholesterol - the devil you know; ceramide - the devil you don't. Trends Pharmacol Sci. 2021; 42(12):1082-1095.
21. Laurila PP, Luan P, Wohlwend M, Zanou N, Crisol B, Imamura de Lima T, Goeminne LJE, Gallart-Ayala H, Shong M, Ivanisevic J, Place N and Auwerx J. Inhibition of sphingolipid de novo synthesis counteracts muscular dystrophy. Sci Adv. 2022; 8(4):eabh4423.
22. Mingione A, Pivari F, Plotegher N, Dei Cas M, Zulueta A, Bocci T, Trinchera M, Albi E, Maglione V, Caretti A, Bubacco L, Paroni R, Bottai D, et al. Inhibition of Ceramide Synthesis Reduces alpha-Synuclein Proteinopathy in a Cellular Model of Parkinson's Disease. Int J Mol Sci. 2021; 22(12).
23. Shiwani HA, Elfaki MY, Memon D, Ali S, Aziz A and Egom EE. Updates on sphingolipids: Spotlight on retinopathy. Biomed Pharmacother. 2021; 143:112197.
24. Dickson RC. Thematic review series: sphingolipids. New insights into sphingolipid metabolism and function in budding yeast. J Lipid Res. 2008; 49(5):909-921.
25. Merrill AH, Jr. Sphingolipid and glycosphingolipid metabolic pathways in the era of sphingolipidomics. Chem Rev. 2011; 111(10):6387-6422.

26. Hannun YA and Obeid LM. Principles of bioactive lipid signalling: lessons from sphingolipids. Nat Rev Mol Cell Biol. 2008; 9(2):139-150.
27. Liu J, Huang X, Withers BR, Blalock E, Liu K and Dickson RC. Reducing Sphingolipid Synthesis Orchestrates Global Changes to Extend Yeast Lifespan. Aging Cell. 2013; 12:833-841.
28. Langfelder P and Horvath S. WGCNA: an R package for weighted correlation network analysis. BMC Bioinformatics. 2008; 9:559.
29. Huang X, Liu J and Dickson RC. Down-regulating sphingolipid synthesis increases yeast lifespan. PLoS Genet. 2012; 8(2):e1002493.
30. MacDonald C, Buchkovich NJ, Stringer DK, Emr SD and Piper RC. Cargo ubiquitination is essential for multivesicular body intralumenal vesicle formation. EMBO Rep. 2012; 13(4):331-338.
31. Stringer DK and Piper RC. A single ubiquitin is sufficient for cargo protein entry into MVBs in the absence of ESCRT ubiquitination. J Cell Biol. 2011; 192(2):229-242.
32. Mulleder M, Capuano F, Pir P, Christen S, Sauer U, Oliver SG and Ralser M. A prototrophic deletion mutant collection for yeast metabolomics and systems biology. Nat Biotechnol. 2012; 30(12):1176-1178.
33. Trapnell C, Williams BA, Pertea G, Mortazavi A, Kwan G, van Baren MJ, Salzberg SL, Wold BJ and Pachter L. Transcript assembly and quantification by RNA-Seq reveals unannotated transcripts and isoform switching during cell differentiation. Nat Biotechnol. 2010; 28(5):511-515.
34. Wang YE, Kutnetsov L, Partensky A, Farid J and Quackenbush J. WebMeV: A Cloud Platform for Analyzing and Visualizing Cancer Genomic Data. Cancer Res. 2017; 77(21):e11-e14.
35. Sherman BT, Hao M, Qiu J, Jiao X, Baseler MW, Lane HC, Imamichi T and Chang W. DAVID: a web server for functional enrichment analysis and functional annotation of gene lists (2021 update). Nuc Acids Res. 2022.
36. Mi H, Muruganujan A, Ebert D, Huang X and Thomas PD. PANTHER version 14: more genomes, a new PANTHER GO-slim and improvements in enrichment analysis tools. Nuc Acids Res. 2019; 47(D1):D419-D426.
37. Brachmann CB, Davies A, Cost GJ, Caputo E, Li J, Hieter P and Boeke JD. Designer deletion strains derived from *Saccharomyces cerevisiae* S288C: a useful set of strains and plasmids for PCR-mediated gene disruption and other applications. Yeast. 1998; 14(2):115-132.
38. Robinson JS, Klionsky DJ, Banta LM and Emr SD. Protein sorting in Saccharomyces cerevisiae: isolation of mutants defective in the delivery and processing of multiple vacuolar hydrolases. Mol Cell Bio. 1988; 8(11):4936-4948.
39. Winzeler EA, Shoemaker DD, Astromoff A, Liang H, Anderson K, Andre B, Bangham R, Benito R, Boeke JD, Bussey H, Chu AM, Connelly C, Davis K, et al. Functional characterization of the *S. cerevisiae* genome by gene deletion and parallel analysis. Science. 1999; 285(5429):901-906.

Figure 1

A

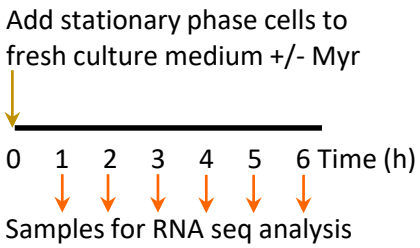

B

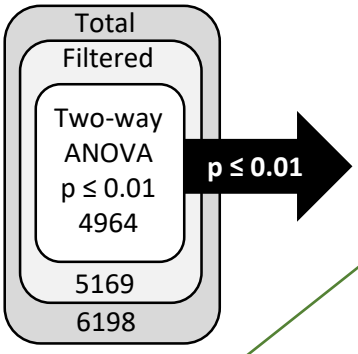

C

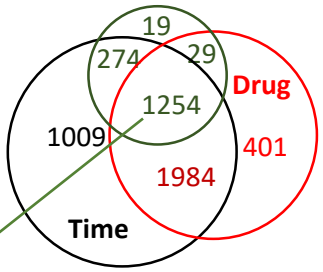

D

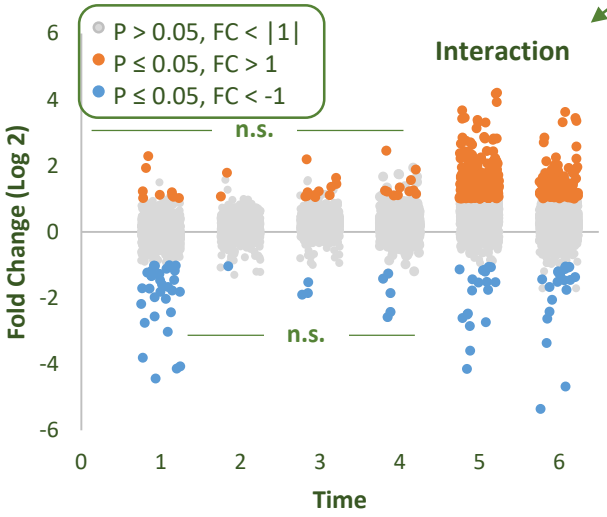

E

High Ranking Terms	Genes	ρ Value
GO:0016020 Membrane	490	7.72E-20
GO:0030479 Actin cortical patch	44	1.67E-17
GO:0055114 Oxidation-reduction process	132	4.09E-13
GO:0005886 Plasma membrane	161	1.22E-11
Sce01100 Metabolic pathways	193	6.68E-11
Sce04144 Endocytosis	39	1.27E-10

Figure 2

A

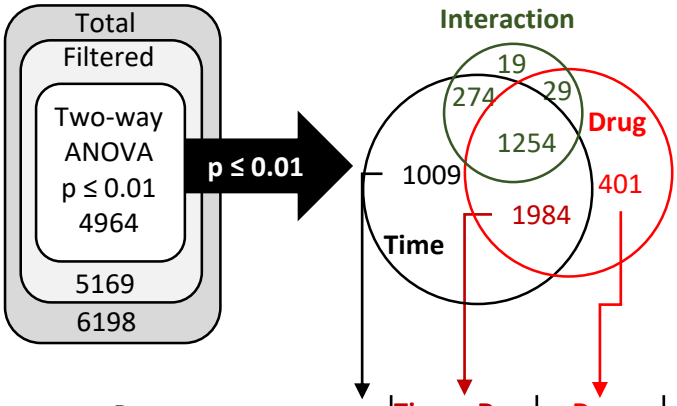

B

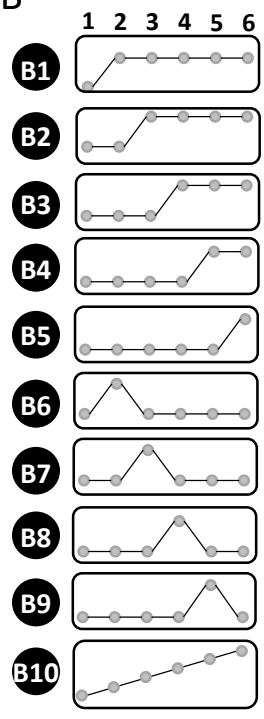

		Time	Time x Drug ↑	Time x Drug ↓	Drug ↑	Drug ↓
B1	+	68	**106***	14		
	-	**269***	**641***	18		
B2	+	21	16	16		
	-	62	**59***	1		
B3	+	36	41	6		
	-	9	5	5		
B4	+	58	**150***	4		
	-	36	13	20		
B5	+	52	**69***	1		
	-	2	0	3	**329***	72
B6	+	51	**63***	4		
	-	24	31	2		
B7	+	3	2	2		
	-	20	23	1		
B8	+	2	3	0		
	-	0	1	0		
B9	+	0	1	0		
	-	1	1	0		
B10	+	**250***	**561***	22		
	-	45	**66***	13		

C

Pattern	Enriched Term	Genes	ρ Value
Venn Sector: Time x Drug (TxD, 1984 genes)			
B1+106	Spindle pole body	15	1.82E-11
	Structural element of cytoskeleton	9	2.77E-08
B1-641	Nucleus	154	4.75E-82
	Ribosome biogenesis	122	9.10E-68
B2-59	DNA repair	8	0.0028
	Cell division	8	0.0034
B4+150	Protein monoubiquitination	6	7.91E-04
	Mitochondrion	46	0.0011
B5+69	Transport	19	0.005
	Endoplasmic reticulum	15	0.0099
B6+63	Ribosome	13	6.89E-07
	Cytoplasmic translation	12	1.57E-06
B10+561	Protein transport	97	4.83E-19
	Transport	140	3.11E-12
B1-66	Nucleolus	16	1.6E-07
	Ribosome biogenesis	14	1.26E-07

D

Venn Sector: Time (T, 1009 genes)			
B1-269	Spindle pole body	10	9.00E-08
	Mitotic nuclear division	11	1.93-06
B10+250	Metabolic pathways	56	9.27E-07
	Glycolytic process	9	8.83E-06

E

Venn Sector: Drug (D, 401 genes)		
Regulation of transcription, DNA-templated	65	3E-10
Nucleus	169	3.85E-09

Figure 3

A

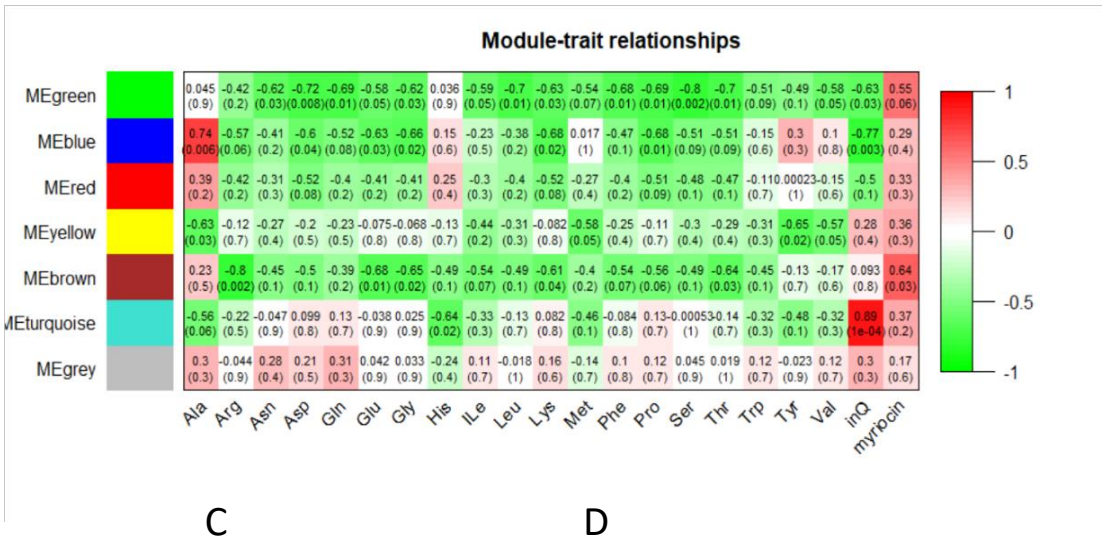

B

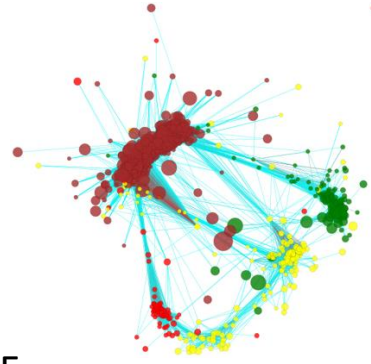

C

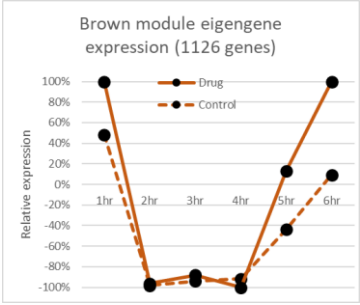

D

Terms (Brown module)	Genes	ρ Value
Regulation of transcription, DNA-templated	180	9.1E-20
Basal transcription factors	20	2.1E-07
RNA transport	33	0.00011
Spliceosome	29	0.00017
Ubiquitin mediated proteolysis	18	0.00254
Arginine and proline metabolism	10	0.00765

E

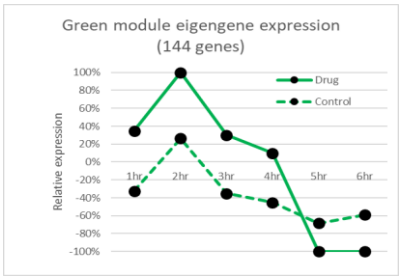

F

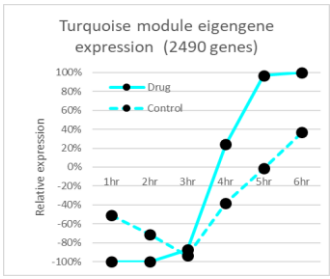

G

Terms (Turquoise module)	Count	ρ Value
GO:0016020~membrane	883	5.7E-26
sce01100:Metabolic pathways	386	1.6E-22
GO:0015031~protein transport	251	1.8E-19
GO:0005739~mitochondrion	611	4.6E-18
GO:0006810~transport	459	1.3E-17
GO:0005789~endoplasmic reticulum membrane	223	8.6E-16

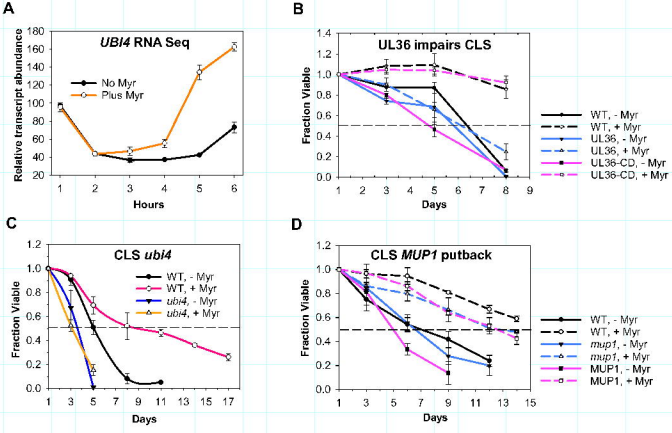
A
UBI4 RNA Seq
Relative transcript abundance
No Myr
Plus Myr
Hours
B
UL36 impairs CLS
Fraction Viable
Days
WT, - Myr
WT, + Myr
UL36, - Myr
UL36, + Myr
UL36-CD, - Myr
UL36-CD, + Myr
C
CLS ubi4
Fraction Viable
Days
WT, - Myr
WT, + Myr
ubi4, - Myr
ubi4, + Myr
D
CLS MUP1 putback
Fraction Viable
Days
WT, - Myr
WT, + Myr
mup1, - Myr
mup1, + Myr
MUP1, - Myr
MUP1, + Myr